Intensity-based adaptive optics with sequential optimization for laser communications

CARLOS E. CARRIZO,[1,2,*] RAMON MATA CALVO,[1] AND ANICETO BELMONTE[2]

[1]*German Aerospace Center (DLR), Institute of Communications and Navigation, 82234 Weßling, Germany*

[2]*Technical University of Catalonia, BarcelonaTech, Department of Signal Theory and Communications, 08034 Barcelona, Spain*

**carlos.carrizo@dlr.de*

Abstract: Wavefront distortions of optical waves propagating through the turbulent atmosphere are responsible for phase and amplitude fluctuations, causing random fading in the signal coupled into single-mode optical fibers. Wavefront aberrations can be confronted, in principle, with adaptive optics technology that compensates the incoming optical signal by the phase conjugation principle and mitigates the likeliness of fading. However, real-time adaptive optics requires phase wavefront measurements, which are generally difficult under typical propagation conditions for communication scenarios. As an alternative to the conventional adaptive optics approach, here, we discuss a novel phase-retrieval technique that indirectly determines the unknown phase wavefront from focal-plane intensity measurements. The adaptation approach is based on sequential optimization of the speckle pattern in the focal plane and works by iteratively updating the phases of individual speckles to maximize the received power. We found in our analysis that this technique can compensate the distorted phasefront and increase the signal coupled with a significant reduction in the required number of iterations, resulting in a loop bandwidth utilization well within the capacity of commercially available deformable mirrors.

OCIS codes: (060.2605) Free-space communication; (110.1080) Adaptive Optics; (030.6140) Speckle.

References and links

1. M. C. Roggemann and B. Welsh, *Imaging Through Turbulence* (CRC University LLC, 1996).
2. L. C. Andrews and R. L. Phillips, *Laser Beam Propagation through Random Media second edition* (SPIE, 2005).
3. K. Saucke, C. Seiter, F. Heine, Mark Gregory, D. Tröndle, E. Fischer, T. Berkefeld, M. Feriencik, I. Richter, and R. Meyer, "The Tesat transportable adaptive optical ground station," Proc. SPIE **9739**, 973906 (2016).
4. M. Li and M. Cvijetic, "Coherent free space optics communications over the maritime atmosphere with use of adaptive optics for beam wavefront correction," J. App. Opt. **54**(6), (2015).
5. M. Li, W. Gao, and M. Cvijetic, "Slant-path coherent free space optical communications over the maritime and terrestrial atmospheres with the use of adaptive optics for beam wavefront correction," J. App. Opt. **56**(2), (2017).
6. M. Li, M. Cvijetic, Y. Takashima, and Z. Yu, "Evaluation of channel capacities of OAM-based FSO link with real-time wavefront correction by adaptive optics," Opt. Express **22**(25), 31337–31346 (2014).
7. M. W. Wright, J. F. Morris, J. M. Kovalik, K. S. Andrews, M. J. Abrahmson, and A. Biswas, "Adaptive optics correction into single mode fiber for a low Earth orbiting space to ground communication link using the OPALS downlink," J. Opt. Soc. Am. **23**(26), (2015).
8. K. E. Wilson, D. Antsos, L. C. Roberts Jr., S. Piazzolla, L. P. Clare, and A. P. Croonquist, "Development of the Optical Communications Telescope Laboratory: A Laser Communications Relay Demonstration Ground Station," in *Proceedings of the International Conference on Space Optical Systems and Applications (ICSOS)*, (2012).
9. K. Murphy, R. Mackey, and C. Dainty, "Branch point detection and correction using the branch point potential method," Proc. SPIE **6951**, 695105 (2008).
10. T. R. Ellis and J. D. Schmidt, "Wavefront Sensor Performance in Strong Turbulence with an Extended Beacon," in *Proceedings of Aerospace Conference* (IEEE, 2010).
11. J. D. Barchers, D. L. Fried, D. J. Link, G. A. Tyler, W. Moretti, T. J. Brennan, and R. Q. Fugate, "The performance of wavefront sensors in strong scintillation," Proc. SPIE **4839**, 217 (2003).

12. K. E. Wilson and L. C. Roberts Jr, "Recent Developments in Adaptive Optics for the LCRD Optical Ground Station at Table Mountain," in *Proceedings of the International Conference on Space Optical Systems and Applications (ICSOS)*, (2014).
13. M. A. Vorontsov, G. W. Carhart, M. Cohen, and G. Cauwenberghs, "Adaptive optics based on analog parallel stochastic optimization: analysis and experimental demonstration," J. Opt. Soc. Am. **17**(8), 1440–1453 (2000).
14. H. Ma, C. Fan, P. Zhang, C. Qiao, and H. Wang, "Adaptive optics correction based on stochastic parallel gradient descent technique under various atmospheric scintillation conditions: numerical simulation," Appl. Phys. B **106**, 939–944 (2012).
15. E. Anzuola, M. Segel, S. Gladysz, and K. Stein, "Performance of wavefront-sensorless adaptive optics using modal and zonal correction," Proc. SPIE **10002**, 100020J (2016).
16. N. Perlot, M. Knapek, D. Giggenbach, J. Horwath, M. Brechtelsbauer, Y. Takayama, and T. Jono, "Results of the optical downlink experiment KIODO from OICETS satellite to optical ground station Oberpfaffenhofen (OGS-OP)," Proc. SPIE **6457**, 645704 (2007).
17. D. Giggenbach, P. Becker, R. Mata Calvo, C. Fuchs, Z. Sodnik, and I. Zayer, "Lunar Optical Communications Link (LOCL): Measurements of Received Power Fluctuations and Wavefront Quality," presented at the International Conference on Space Optical Systems and Applications (ICSOS), Kobe, Japan, 7–9 May. (2014).
18. M. A. Vorontsov, "Decoupled stochastic parallel gradient descent optimization for adaptive optics: integrated approach for wave-front sensor information fusion," J. Opt. Soc. Am. **19**(2), 356– 368 (2002).
19. Q. Fu, J. Pott, F. Shen, and C. Rao, "Stochastic parallel gradient descent optimization based on decoupling of the software and hardware," J. Opt. Communications **310**, 138–149 (2014).
20. Zhao Fang, "Plane wave coupling into single-mode fiber in the presence of random angular jitter," J. App. Opt. **48**(27), 5184–5189 (2009).
21. A. Belmonte and J. M. Kahn, "Capacity of coherent free-space optical links using atmospheric compensation techniques," Opt. Express **17**(4), 2763–2773 (2009).
22. J. W. Goodman, *Introduction to Fourier Optics* (McGraw-Hill, 1996), Chap. 3.
23. T. Nguyen, H. Majeed, and G. Popescu, "Plane-wave decomposition of spatially random fields," Opt. Lett **40**(7), 1394–1397 (2015).
24. J. W. Goodman, *Speckle Phenomena in Optics: Theory and Applications* (Roberts & Company, 2007).
25. EM Fields and Waves, "Angular spectrum representation," (Photonics Laboratory ETH Zurich, 2016), https://www.photonics.ethz.ch/fileadmin/user_upload/Courses/EM_FieldsAndWaves/AngularSpectrumRepresentation.pdf.
26. I. Freund and N. Shvartsman, "Structural correlation in Gaussian random wave fields," Phys. Rev. E **51**, 3770 (1995).
27. A. Belmonte and J. M. Kahn, "Sequential Optimization of Adaptive Arrays in Coherent Laser Communications," J. Lightwave Technol. **31**(9), 1383–1387 (2013).
28. A. Belmonte and J. M. Kahn, "Performance of synchronous optical receivers using atmospheric compensation techniques," Opt. Express **16**(18), 14151–14162 (2008).
29. N. A. Roddier, "Atmospheric wavefront simulation using Zernike polynomials," Opt. Eng. **29**(10), 1174–1180 (1990).
30. R. Noll, "Zernike polynomials and atmospheric turbulence," J. Opt. Soc. Am. **66**(3), 207–211 (1976).
31. Boston Micromachines Corporation, "The Kilo-DM: A high performance wavefront corrector for demanding applications in astronomy, laser communications and long-range imaging", http://www.bmc.bostonmicromachines.com/pdf/Kilo-DM.pdf.

1. Introduction

Free-space optical communication (FSOC) is rapidly becoming a key enabling technology for terrestrial, aerial, and space communication networks. However, laser communication through the atmosphere is challenging because turbulence disturbs the received phase wavefront and develops into signal fading, reducing the communications performance [1,2]. Adaptive optics (AO) techniques, based on deformable mirrors (DM) and acting over single-aperture receivers, are used to improve the performance of laser communication links by mitigating the consequences of atmospheric turbulence [3–6].

The main motivation of AO compensation in FSOC is the feasibility of achieving very high data rates, which requires an efficient single mode fiber (SMF) coupling. As long as the turbulence level is moderate, traditional AO systems perform satisfactorily. The most common AO approach is based on the well-known Shack-Hartmann wavefront sensor. Using this technique, successful optical downlinks achieving Gigabits data rates under weak to moderate turbulence have been recently demonstrated [3–8]. However, under the regime of strong turbulence, Shack-Hartmann-based solutions may fail to guarantee a stable fiber coupling. For instance, in low-earth-orbit (LEO) satellite downlinks, strong turbulence may

induce intense scintillation and phase wavefront singularities (branch points), thus, seriously limiting the performance of such sensor [9–12].

Indirect wavefront sensing techniques have gained more scientific attention in the field of FSOC [13–15], mainly due to improvements associated with fast DMs, parallel processing, and efficient blind search algorithms [15]. These sensor-less techniques iteratively optimize the received power, updating the AO phase compensation system based on the analysis of a performance metric, which is generally power in the bucket. Two different blind search approaches are usually considered. The zonal approach randomly changes the states of single DM actuators in searching for optimal power coupling; the modal approach shapes all actuators at once, following an orthogonal modal basis (e.g., Zernike polynomials) [15]. In general, indirect phase sensing benefits from simple optical setups, high power efficiency, and robustness against power scintillation.

Unfortunately, indirect wavefront sensing techniques also have limitations when dealing with laser propagation through the atmosphere. In particular, the short coherence time of the field fluctuations may overcome the correction capacity of iterative techniques, where usually hundreds of iterative measurements may be required [15]. Considering a typical LEO downlink, where coherence times of one millisecond are usual [16,17], unpractical control bandwidth above $100\,\mathrm{kHz}$ may be required. Recent hybrid phase measurement techniques, considering both direct and indirect methods simultaneously [18,19], may reduce the required control bandwidth by half but at the expense of increasing the complexity of the optical setup.

In this paper, we address the difficulties and limitations described above and propose a different iterative wavefront sensing approach that can achieve an efficient SMF coupling in strong atmospheric conditions. Our method uses segmented mirror phasing and considers focal-plane intensity measurements to drastically reduce the required number of iterations. The adaptation approach is based on sequential optimization of the speckle pattern in the focal plane and works by iteratively updating the phases of individual speckles to maximize the received power.

The remainder of this paper is organized as follows. In Section 2, the system and principal mathematical terms are described. In Section 3, the fundamental theoretical concepts and adaptation method are detailed. In Section 0, a numerical analysis of its performance under realistic turbulence conditions is discussed. Finally, the concluding remarks are presented in Section 4.

2. Turbulence compensation system

A simplified scheme of the hypothetical optical receiver is shown in Fig. 1.

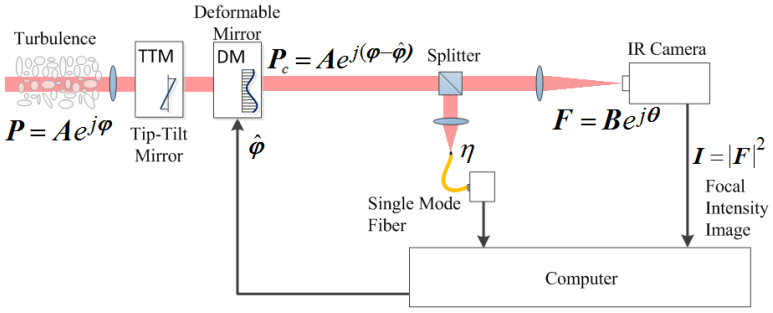

Fig. 1. Simplified scheme of the optical receiver. The incoming beam is corrected in tilt, reflected in the deformable mirror, and focused on an infrared camera and single mode fiber. The speckle image and feedback coupled power are used to sequentially compensate the distorted phasefront via the iterative control of the deformable mirror.

When a laser beam passes through the turbulent atmosphere, the wavefront $\boldsymbol{P} = \boldsymbol{A}\exp(j\boldsymbol{\varphi})$ is affected by distortions in amplitude $\boldsymbol{A}$ and phase $\boldsymbol{\varphi}$. Here, the two-dimensional spatial fields are indicated by bold letters. In the receiver, the distorted beam is captured by a single monolithic aperture, guided to the tip-tilt mirror (TTM) for angle-of-incidence correction, and reflected in the deformable mirror (DM). The DM modifies its shape according to an estimated phase map $\hat{\boldsymbol{\varphi}}$, inducing phase-only variations on the wavefront $\boldsymbol{P}$, and resulting in a phase-compensated reflected beam $\boldsymbol{P}_{\mathrm{c}} = \boldsymbol{A}\exp\left(j\left(\boldsymbol{\varphi} - \hat{\boldsymbol{\varphi}}\right)\right)$.

Here, $\hat{\boldsymbol{\varphi}}$ is defined by an iterative algorithm requiring two inputs. The first input is a focal intensity image $\boldsymbol{I} = |\boldsymbol{F}|^2$ captured by a camera sensor. The complex field $\boldsymbol{F} = \boldsymbol{B}\exp\left(j\boldsymbol{\theta}\right)$, with amplitude $\boldsymbol{B}$ and phase .., results from the optical Fourier transform of $\boldsymbol{P}_{\mathrm{c}}$. The second input is a real-time acquisition of the power coupled into a single mode fiber. The coupled power is defined by the SMF coupling efficiency η, which is calculated in the pupil plane as [20,21]

$$\eta = \frac{\left|\int \boldsymbol{P}_{\mathrm{c}}(r)^{*}\boldsymbol{U}_{0}(r)\mathrm{ds}\right|^{2}}{\int\left|\boldsymbol{P}_{\mathrm{c}}(r)\right|^{2}\mathrm{ds}\cdot\int\left|\boldsymbol{U}_{0}(r)\right|^{2}\mathrm{ds}}, \tag{1}$$

where, complex conjugate is indicated by $*$ and $\boldsymbol{U}_{o} = \sqrt{2/\left(\pi w_{\mathrm{a}}^{2}\right)}\exp\left(-\left(r^{2}/w_{\mathrm{a}}^{2}\right)\right)$ is the power-normalized, back propagated mode of a single-mode fiber with $1/e$ mode field radius w_0. Here, $w_{\mathrm{a}} = \lambda f/\left(\pi w_0\right)$ is the mode field radius, λ is the laser wavelength, and f is the focal length of the coupling lens.

3. Method

Whenever power measurements are made, phase information of the optical field is lost and the distorted wavefront $\boldsymbol{P}$ in Fig. 1 cannot be completely recovered from the CCD intensity image $\boldsymbol{I}$. Nonetheless, with the appropriate pupil field representation, the focal image can provide useful phase information to increase the convergence rate of an iterative AO approach.

In Fourier optics, a wavefront can be described by the sum of an infinite number of plane waves oriented in different directions in space, each one carrying a part of the total energy of the field. After the wavefront passes through a lens, the energy of each plane wave converges in a unique non-equal point in the focal plane. This focal plane is known as the Fourier transform plane, where the wavefront is transformed into spatial frequency spectra [22]. When a distorted wavefront is considered, measurements of intensity in the focal plane show fine-scale fluctuations in space, i.e., speckles. These speckles appear because the wavefront is composed of a multitude of independent complex plane waves having both random amplitude and random phase. An extensive analysis of the plane wave decomposition of intensity focal speckles can be seen in [23].

A wavefront affected by turbulence experiences different amounts of phase delays [24]. Similar phase delays in the pupil define coherent regions in the phasefront. In Fig. 2(a), areas of the same color represent the regions where the phase remains coherent. From the theory of angular spectrum of plane waves [22,25], we assume that each coherent region in the pupil plane becomes a source of plane waves with similar propagation directions, focusing in a well-defined area in the focal plane. The contribution of this set of plane waves, with slight differences in the propagation direction, results in a speckle with a well-defined maximum of intensity. Additional speckles are produced by a different set of plane waves associated with other coherent regions in the pupil, see Fig. 2(b). At this point, we first assume that each coherent region in the pupil phase, which is related to a focal speckle, can be represented by a

single plane wave. Second, the amplitude of the plane wave is defined by the peak intensity of the associated speckle, as it represents the ensemble contribution of all the plane waves of the coherent region, see Fig. 2(c). Therefore, in this analysis, the distorted wavefront $\boldsymbol{P}$ can be conveniently approximated by a finite set of M plane waves, where each one is related to one of the M main focal speckles. In this case, the wavefront can be described as

$$\boldsymbol{P} \approx \sum_{l=1}^{M} b_l \exp\left(j\theta_l\right)\exp\left(j\boldsymbol{k}_l\ \boldsymbol{r}_l\right). \tag{2}$$

Each plane wave in Eq. (2) has a scalar amplitude $b_l \in$, a scalar phase shift $\theta_l \in$, and a propagation direction given by the wave vector $\boldsymbol{k}_l$ [23]. Additionally, each plane wave results in an independent speckle spot at the coordinate $\boldsymbol{r}_l$ of the intensity pattern $\boldsymbol{I}$ in the focal plane [26].

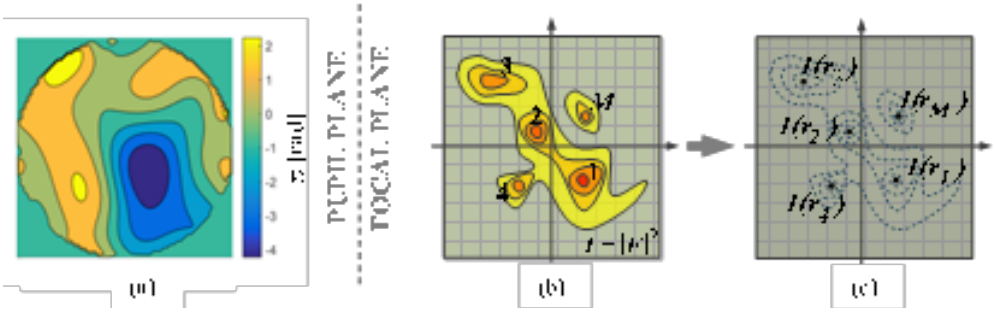

Fig. 2. (a) Representation of the coherent regions of phase in the pupil plane, delimited by phase differences of π radians. (b) Representation of the focal intensity image with M main speckles. (b) Simplification with the M peak intensities.

Figure 3 details the adaptation process and the algorithm considered in this analysis. It involves three main steps: laser speckle imaging and selection of the M most intense speckle spots in the focal plane; identification of the corresponding M plane waves in the pupil plane; and optimization of the M independent random phases.

In the first step of the method, an image of the focal intensity $\boldsymbol{I}$ is captured with the camera and square rooted to obtain amplitude coefficients $b_l = \sqrt{\boldsymbol{I}(\boldsymbol{r}_l)}$. The M main speckles coordinates are detected using image processing based on the search of local maximas and classified in descending order based on their peak amplitudes b_l. The result is an array of coefficients $b = [b_1, b_2, b_3, ..., b_M]$ that are associated with sensor coordinates $\boldsymbol{r} = [\boldsymbol{r}_1, \boldsymbol{r}_2, \boldsymbol{r}_3, ..., \boldsymbol{r}_M]$, respectively. In Fig. 3, this is represented as a set of images, each one with a single component of amplitude b_l at the coordinate $\boldsymbol{r}_l$ of the speckle maximum.

The second step involves identifying the M plane waves in the pupil plane corresponding to the M selected speckle spots in the focal plane. Each l plane wave has a propagation direction that is completely identified by a propagation vector $\boldsymbol{k}_l$, see Eq. (2). In Fourier optics, a deviation in the direction a wave of light propagates is a tilt, and tilt angles can be used to quantify the slope of a phase profile across the pupil of an optical system. Consequently, the identification of the propagation directions of the M waves is performed by linking a specific tilt angle in the pupil with the corresponding speckle spot in the focal plane. In this way, each $l \in \{1, 2, 3, ..., M\}$ detected speckle, with coordinate $\boldsymbol{r}_l$ and amplitude coefficient b_l, as measured by the CCD camera in the focal plane, will be associated to a

well-defined tilted phase profile of a plane wave in the pupil plane. Note that no Fourier transform of the intensity speckle distribution is required.

In the third step, the method estimates and compensates the distorted pupil phasefront $\boldsymbol{\varphi}$. This process requires adding up the identified M plane waves, calculating the argument of the summation $\hat{\boldsymbol{\varphi}}$, and using this resultant phase to shape the DM, see Fig. 1. However, the impossibility of measuring the necessary phase shifts θ_l of the plane waves requires an iterative estimation of each optimum $\hat{\theta}_{\text{opt}}$.

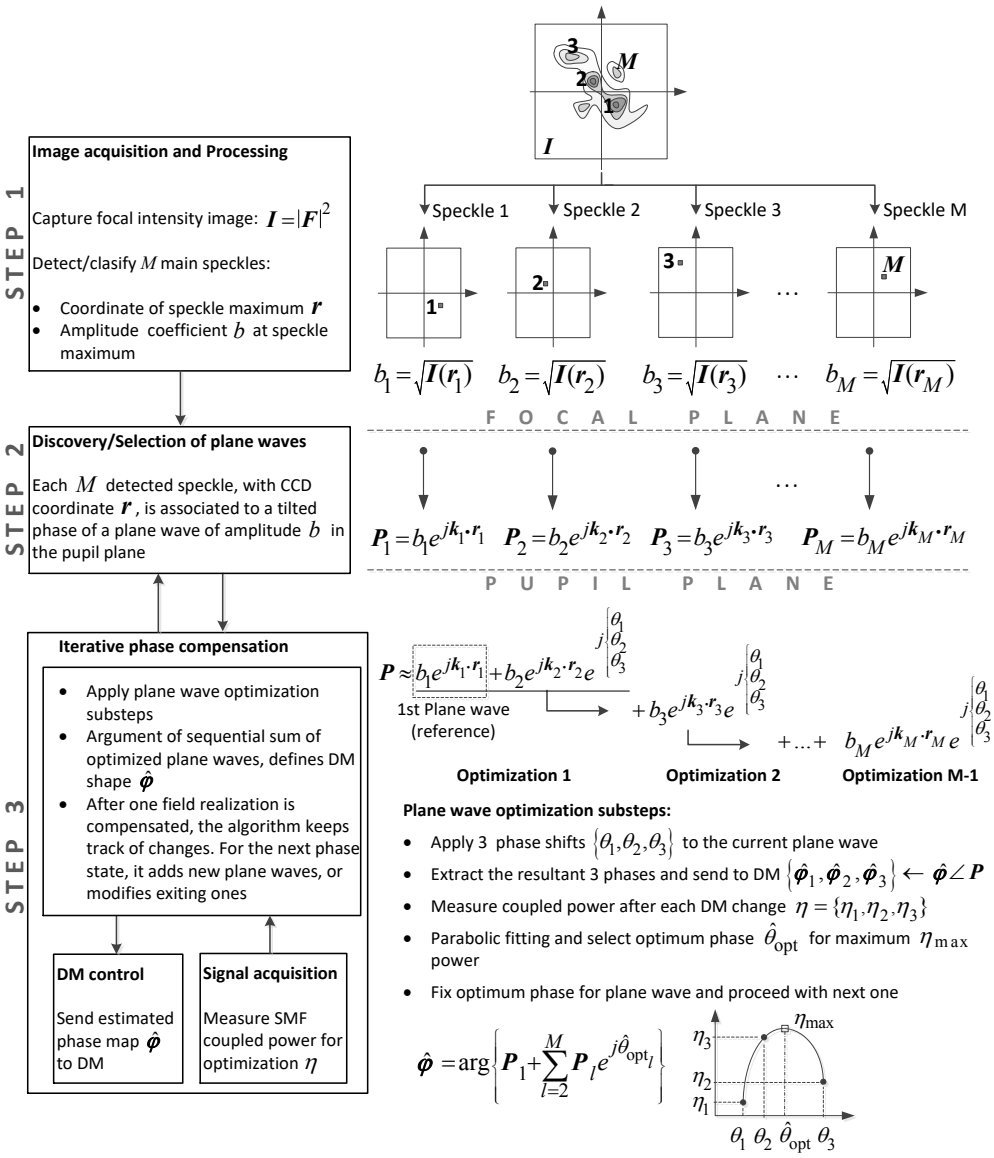

Fig. 3. Adaptation algorithm. The captured intensity image is used to create a set of pupil plane waves, each one associated with a main focal speckle. The plane waves are sequentially combined after the optimization of their respective phase shifts, which is done using the feedback power coupling. The argument of the optimized plane wave summation is applied to the DM and represents the estimated distorted phasefront.

Instead of a blind search, our method can obtain these phase shift estimates in a closed form via the optimization of a quadratic cost function based on the measured power coupling. Because quadratic optimization problems are always convex, three measurements are enough to discover the optimum phase shift of each plane wave.

As depicted in step 3 of Fig. 3, the method always considers the first plane wave as an initial reference from which the field will further evolve. Note that no phase shift is required here. In order to find the optimum phase shift of the second plane wave $\hat{\theta}_{\text{opt2}}$, the method shifts the phase of such a plane wave with three scalar phase settings $\theta = \{\theta_1, \theta_2, \theta_3\}$ and calculates the argument of the summation, so as three estimated pupil phases $\hat{\boldsymbol{\varphi}} = \{\hat{\boldsymbol{\varphi}}_1, \hat{\boldsymbol{\varphi}}_2, \hat{\boldsymbol{\varphi}}_3\}$ are obtained. Shaping the DM with these phases has an instantaneous effect on the power coupled into the single mode fiber. Thus, three optical powers $\eta = \{\eta_1, \eta_2, \eta_3\}$ are measured concurrently with each DM change, one for each pupil phase. The final stage requires a parabolic fitting of these measured values, finding the optimum phase shift $\hat{\theta}_{\text{opt2}}$ at the position of the maximum coupling $\eta_{\max}$. Repeating this procedure on the subsequent plane waves results in an optimal adaptation array $\hat{\theta}_{\text{opt}} = \{\hat{\theta}_{\text{opt2}}, \hat{\theta}_{\text{opt3}}, ..., \hat{\theta}_{\text{optM}}\}$, where each component is an optimum phase shift of its associated plane wave.

Note that a continuous variation of the scalar phase shift θ in Eq. (2) results in an oscillation of the coupled power η, which varies following a phase-shifted cosine function. Consequently, to obtain the quadratic cost function of the optimization process, the values of θ need to be constrained to a range of π. We assign the values of $\theta = \{\pi/100, \pi/3, 2\pi/3\}$ linearly and equally spaced, using the same values for each optimization. When the $\hat{\theta}_{\text{opt}}$ matches a minimum of the cosine function, the maximum can be located at $\hat{\theta}_{\text{opt}} + \pi$. Here, power variations will depend on the θ spacing. Consequently, the first set of plane wave optimizations will show higher power excursions, while the subsequent optimizations will be performed around the anterior optimums, thus, reducing the variation of the coupling power. This is essential for the dynamic regime and considers gradual speckle evolution in a temporal scale of the coherence time of the field.

The iterative phase compensation method described above follows a standard coordinate-wise ascent algorithm. The convexity property always allows the algorithm to find a global, although not necessarily unique, solution. The orthogonality of the plane waves implies that the algorithm can indeed construct the optimum phase shift array by optimizing each plane wave individually. For our power maximization problem, the coordinate-ascend approach relies on the fact that the total optical power in the focal plane is a linear superposition of the energy contributions from all M plane waves. This means that each optimized plane wave increases the overall power coupling.

Interestingly, from the focal plane perspective, this adaptation scheme is equivalent to modify the phases of the associated speckle spots at the focal plane instead of the pupil plane, so as their sum improves the composite optical signal [27]. Additionally, it is important to remark that the method only requires $N_{\text{iter}} = 3(M-1)+1$ power measurements. This number can be considered to actively manage the loop bandwidth utilization under different turbulence conditions.Numerical performance

We illustrate the performance profiles offered by the proposed adaptation approach when a practical optical fiber receiver, set with adaptive optics, confronts a typical atmospheric turbulence condition. We conducted a numerical analysis, and the following set of experiments was performed on synthetically built optical signals. It considers compensation

of M speckle spots and assumes that a single aperture contains a lens that couples the received light into a single-mode optical fiber.

In order to synthesize the optical signals, we assume Kolmogorov turbulence [1] and quantify the atmospheric turbulence strength by the normalized aperture diameter D/r_0. Here, D is the aperture diameter of the single receiver system, and the wavefront coherence diameter r_0 describes the statistical spatial coherence of the wavefront in the receiver plane. For a fixed aperture diameter, as coherent diameter decreases, turbulence reduces the SMF coupling efficiency. This phenomenon is typical in FSOC from LEO satellites, where the elevation changes during the satellite pass. For this analysis, we consider strong turbulence with a $D/r_0 = 10$, having $r_0 \approx 4$ cm and $D = 40$ cm. This reflects a realistic condition of a LEO downlink at $5°$ elevation from the horizon, as shown in [5,16,17].

To simulate the effects of the turbulent propagation scenario, we numerically synthesize a sufficiently large number of statistically uncorrelated phase wavefronts. We consider only the phase fluctuations of the field as the dominant factor affecting the fiber coupling efficiency [28,15]. Thus, we use the single-screen phase method to impress the phase distortion into the optical signal. This method, described in [29,30], is simple to implement and allows fast generation of a large number of fields. To create each phase screen, a set of weighted Zernike polynomials is combined. For the weights, an equal number of Karhunen-Loève coefficients is generated using the diagonalized covariance matrix of the Zernike polynomials. In our analysis, we use not less than 600 polynomials for an accurate statistical generation of each phase front.

Each wavefront is created with a size of $256x256$ pixels and a sampling spacing of 1.56 millimeters. This considers a received laser wavefront captured by the 40 cm telescope aperture. To obtain the focal image with sufficient speckle resolution, each wavefront is zero padded and then Fourier transformed. The size of the focal image, which represents the size of the CCD, is $256x256$ pixels. The simulation considers a minimum of $7x7$ pixels for resolving the minimum speckle size, which corresponds to the Airy pattern diameter when its intensity falls to $1/e^2$. The compensation of the distorted phase is performed ideally without special consideration of a specific DM.

Figure 4 shows (a) the mean SMF coupling efficiency and (b) the normalized variance of the received signal as a function of the number of compensated speckle spots and the number of signal photons collected on the receiver aperture.

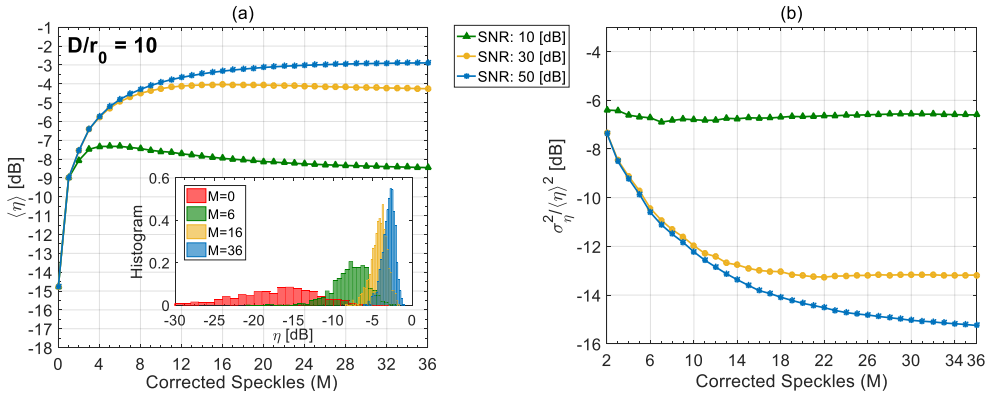

Fig. 4. (a) mean SMF coupling efficiency and (b) normalized variance of the received signal as a function of the number of corrected speckle spots and the signal to noise ratio of the optimization signal (SNR). The inset shows the normalized histogram at the maximum of each curve.

For an optical receiver whose dominant noise source is shot noise, the signal SNR can be taken as the number of signal photons collected by the input aperture.

Without a strong impact of the noise, due to generally higher peak intensity level, the tilt correction of the first speckle in Fig. 4(a) greatly increases the coupled power. For the case of $\mathrm{SNR} = 50\,\mathrm{dB}$, the correction of additional speckles $M \geq 2$ improves the fiber coupling efficiency until a plateau is reached. At this point, the correction of further speckles with lower intensity does not significantly contribute to the overall coupling. The same behavior is seen in Fig. 4(b), where the normalized variance rapidly falls to a plateau for $M \geq 36$. Instead, with lower $\mathrm{SNR} = [30,10]\,\mathrm{dB}$, noise-induced deviations of the coupling power affect the phase shift optimization process, penalizing the coupling gain and limiting the reduction of the variance. Note that keeping this variance minimal is a key factor for error-free data links in the FSOC scenarios. Furthermore, the performance with low SNR is dependent on the number of corrected speckles. The curves of $\mathrm{SNR} = 30\,\mathrm{dB}$ and $10\,\mathrm{dB}$, in Fig. 4(a), show maximums at $M \approx 16$ and $M \approx 6$, respectively, and negative slopes with increasing number of corrected speckles. After these maximums, the signal noise has a greater effect in the optimization of plane waves associated to speckles of lower intensity. This leads to suboptimal phase shifts and propagates errors, which affects the subsequent optimizations and reduces the overall performance. The optimum number of speckles to be corrected can be approximated as $M_{\mathrm{opt}} = 0.54\mathrm{SNR}$ for $10 \leq \mathrm{SNR} \leq 50\,[\mathrm{dB}]$. For a SNR of $50\,\mathrm{dB}$ and higher, the coupling efficiency always improves by adding newly corrected speckles.

The inset of Fig. 4(a) depicts the normalized histogram of the coupling efficiency at the maximum of each curve, where the fields are corrected with the above mentioned $M = [6,16,36]$. Even though the described penalties in the performance exist, an improvement in gain and variance compared to the absence of AO compensation $M = 0$ can be appreciated.

As previously mentioned, all plane waves can be optimized individually and then combined to reconstruct the distorted phasefront. It is not strictly necessary to start the process with the speckle of higher intensity. However, by first optimizing the speckle of higher intensity and following the described sequence, we obtain a significant initial improvement in the coupling efficiency. This increases the SNR and reduces the impact of the noise in the optimization of subsequent speckles of lower intensity.

Regarding the bandwidth utilization, the method significantly reduces the required number of iterations compared to the iterative systems based on a stochastic approach. This is possible because it directly addresses the speckles of higher intensity, optimizing each associated plane wave with just three iterations. Generally, it is considered that the number of focal speckles produced by a distorted field is approximately equal to $(D/r_0)^2$. Since the intensity distribution of a fully-developed speckle pattern can be described as negative exponential [24], only a few speckles contribute significantly to the improvement of the coupling efficiency. In Fig. 4, the higher coupling improvement happens with the first corrected speckles, which contain most of the focal intensity. At this point, the versatility of this method is worth to mention. For a typical coherence time of the field of 1 millisecond [16,17], and allowing $1\,\mathrm{dB}$ penalty from the maximum coupling efficiency, this method requires a loop bandwidth utilization of 30 kHz to achieve a coupling efficiency of $-4\,\mathrm{dB}$ with 28 iterations (10 corrected speckles). This bandwidth requirement is well within the reach of commercially available DMs [31].

On the other hand, our method requires image processing and thus, additional time has to be taken into account. Here, the use of the local maxima algorithm for the detection and posterior classification of multiple speckles delivers higher precision and more stable results as compared to a centroid-based alternative. Even though this task can be carried out in a time

scale on the order of 100 microseconds, parallel processing is a must. This means that by the time the DM has performed all the initial iterations, the image processing and plane wave selection of the next field state need to be ready. Since high frame rate DMs [31] use buffers to pre-load the phase maps before shaping the mirror, this is possible but a specific control algorithm needs to be developed accordingly. A continued tracking of the evolving speckles is essential to anticipate the new set of plane waves and maintain the correction dynamically. Overall, the benefits of the bandwidth reduction come at the expense of relatively more complexity in the algorithm and control. Extensive experimental work is being carried out to address these technical aspects.

4. Conclusions

We have concluded that our adaptation process is a valid alternative to the conventional iterative adaptive optics approach to achieve efficient single-mode power coupling in FSOC scenarios. We have discussed a novel phase-retrieval technique that indirectly determines the unknown phase wavefront from the focal-plane intensity measurements and an adaptation approach that is based on the sequential compensation of the distorted pupil phasefront. The technique works by iteratively updating the phases of individual speckles to maximize the received power coupled into a single-mode fiber. We found that instead of conventional iterative phase compensation systems, the sequential phase retrieval technique combined with the focal intensity measurements is a more flexible approach to increase signal coupling to the receiver.

The main strength of the method is its capacity of drastically reducing the total bandwidth utilization of the adaptive optics system. This improvement is possible by operating only on the speckles of higher intensity. As a result, the method shows versatility regarding bandwidth utilization, with the capacity of being dynamically controlled depending on the turbulence strength, while providing significant coupling gain, as well as improved signal stability, even under challenging turbulent propagation conditions.